

# 1 **Rapidly Changing Lake-Terminating Glaciers in High** 2 **Mountain Asia: A Dataset from 1990 to 2022**

3 Yunyi Luo<sup>1,2</sup>, Qiao Liu<sup>1</sup>, Xueyuan Lu<sup>1,2</sup>, Yongsheng Yin<sup>1,2</sup>, Jiawei Yang<sup>1,2</sup>, Xuyang  
4 Lu<sup>1</sup>

5 1 Institute of Mountain Hazards and Environment, Chinese Academy of Sciences, Chengdu 610041,  
6 China.

7 2 College of Resources and Environment, University of Chinese Academy of Sciences, Beijing 100049,  
8 China

9 Correspondence: Qiao Liu; liuqiao@imde.ac.cn

10 **Abstract.** Lake-terminating glaciers (LTGs) typically exhibit higher rates of retreat and thinning  
11 compared to land-terminating glaciers. However, a comprehensive inventory for LTGs and their  
12 associate proglacial lakes across High Mountain Asia (HMA) is currently lacking, limiting further  
13 understanding of their spatial heterogeneity in glacier change. This study employs a semi-automated  
14 identification method, coupled with rigorous visual inspection, to construct a comprehensive inventory  
15 of LTGs and proglacial lakes in HMA for 1990 and 2022. Our data indicate that, by 2022, HMA hosted  
16 1740 LTGs ( $5082.08 \pm 13.15 \text{ km}^2$ ), among which 667 glaciers ( $3454.59 \pm 12.43 \text{ km}^2$ ) remained in contact  
17 with proglacial lakes since 1990, 1073 ( $1627.49 \pm 4.30 \text{ km}^2$ ) are newly developed and 468 ( $960.13 \pm$   
18  $3.18 \text{ km}^2$ ) had disconnected from proglacial lakes during the investigation period. Accordingly, 645  
19 proglacial lakes ( $207.18 \pm 0.82 \text{ km}^2$ ) remained in contact with ice, 1123 new lakes ( $54.85 \pm 0.35 \text{ km}^2$ )  
20 formed, and 485 lakes ( $45.31 \pm 0.34 \text{ km}^2$ ) detached from ice (including 25 disappeared). During the past  
21 32 year, the total area of proglacial lakes increased by  $138.19 \pm 1.18 \text{ km}^2$  (81.7%), alongside a glacier  
22 area loss of  $324.43 \pm 19.23 \text{ km}^2$  (5.1%). The southern regions of HMA, particularly the Hindu Kush,  
23 Himalayas, Nyainqentanglha, and Gangdise Mountains, exhibiting the highest concentration and rapidest  
24 changes of the glacier-lake system. We hope that this dataset will improve our understanding of mountain  
25 glacier-lake interactions, water availability, as well as glacier-related hazards in HMA.

26 The dataset is openly available in GeoPackage format, with full attribute tables compliant with the RGI  
27 7.0 vocabulary, and is hosted on Zenodo at <https://doi.org/10.5281/zenodo.17369580> (Luo and Liu,  
28 2025).

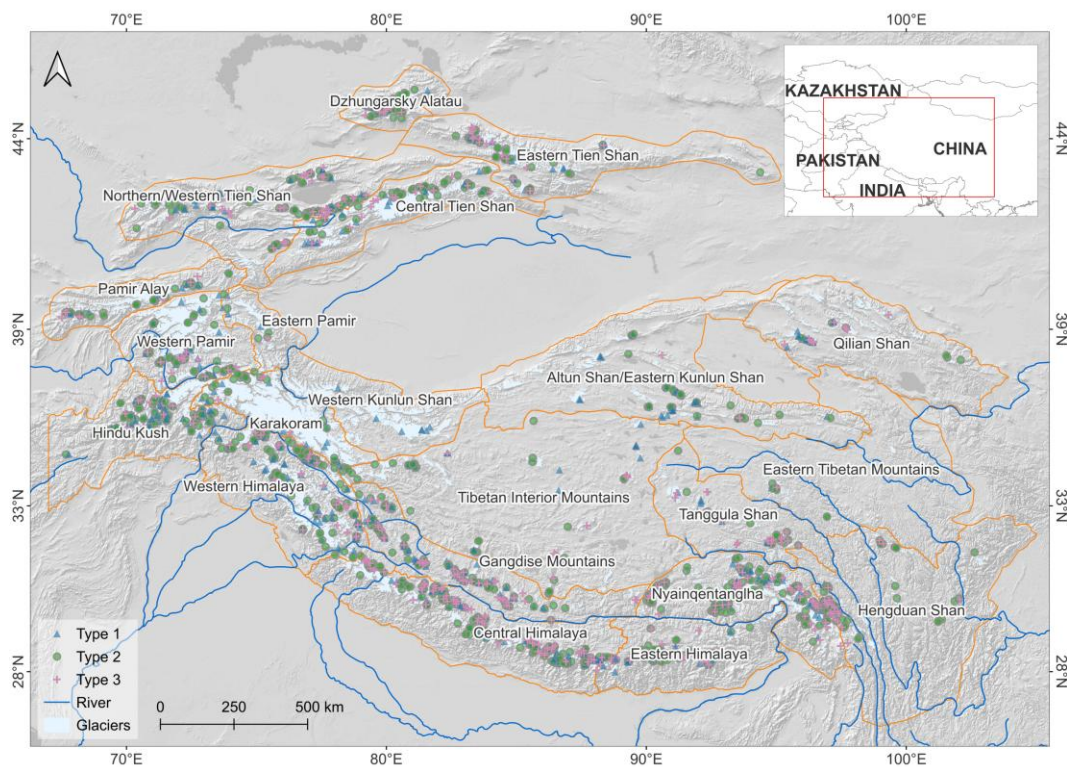
## 29 **1 Introduction**

30 Proglacial lakes in direct contact with glacier termini play a critical role in glacier evolution (Liu et  
31 al., 2020; Truffer and Motyka, 2016; Chernos et al., 2016) and are a primary driver of spatial  
32 heterogeneity in glacier responses to climate change (Brun et al., 2019; Maurer et al., 2019). Proglacial  
33 lakes typically form behind end or lateral moraines, on debris-covered glaciers often developed through  
34 the coalescence of multiple supraglacial ponds near the glacier terminus (Carrivick and Tweed, 2013;  
35 Quincey et al., 2007; Mertes et al., 2017). The influence of lake water on glacier change operates  
36 primarily through two mechanisms: (1) thermal undercutting by lake water (Truffer and Motyka, 2016)  
37 and calving at the glacier front (Benn et al., 2007a), which together accelerate subaquatic and frontal  
38 ablation; and (2) when glacier termini come into contact with sufficiently deep water, the buoyancy of  
39 the lake reduces basal effective pressure, thereby enhancing glacier flow and dynamic thinning  
40 (Sugiyama et al., 2011; Sutherland et al., 2020; Benn et al., 2007b). Observations indicate that LTGs in  
41 High Mountain Asia (HMA) have mass loss rates 18–97% higher than the regional average (Brun et al.,  
42 2019) , and under comparable geographic conditions, their surface velocities are typically two- to  
43 threefold greater than those land-terminating counterparts (Pronk et al., 2021; Tsutaki et al., 2019).  
44 Furthermore, Zhang et al. (2023) reported that existing geodetic methods, by failing to account for the  
45 replacement of glacier ice by lake water, underestimate the mass loss of Himalayan LTGs by  
46 approximately 6.5%.

47 HMA encompassing the entire Tibetan Plateau and its surroundings contains the largest  
48 concentration of mid-latitude mountain glaciers on Earth. Driven by ongoing global warming, glaciers  
49 in HMA have undergone a persistent negative mass balance, with an average mass loss rate of  $-20.1 \text{ Gt}$   
50  $\text{a}^{-1}$  during 2000–2019 (Hugonnet et al., 2021). Glacier meltwater has driven substantial runoff and  
51 facilitated the formation and expansion of glacial lakes. From 1990 to 2018, the number of glacial lakes  
52 in HMA increased by 11%, and their total area expanded by 15% (Wang et al., 2020). The ongoing  
53 increase in both the number and extent of proglacial lakes underscores the critical need for a  
54 comprehensive assessment of lake-terminating glacier-proglacial lake systems in HMA. Such an  
55 evaluation is essential for elucidating feedback between the lake and ice, forecasting their responses to  
56 future climate change, and informing evidence-based strategies for water resource management and

57 disaster risk mitigation. Although several regional-scale glacial lake inventories have been published in  
 58 recent years (Wang et al., 2020; Chen et al., 2021; Zhang et al., 2015; Worni et al., 2013; Salerno et al.,  
 59 2012; Shugar et al., 2020), most datasets do not distinguish the contact status and its change between  
 60 glaciers and proglacial lakes. Moreover, there is currently no comprehensive inventory of lake-  
 61 terminating glacier-proglacial lake systems covering the entire HMA, and their spatiotemporal evolution  
 62 remains poorly understood. Therefore, this study aims to construct a dataset of LTGs and proglacial lakes  
 63 for HMA based on multi-source remote sensing data, thereby filling this research gap and providing  
 64 fundamental database to support studies on regional glacier change, water resource assessment, disaster  
 65 management, and glacier hydrology.

## 66 2 Study area



67  
 68 **Figure 1. Location of HMA and distribution of LTGs. Glacier outlines from the Randolph Glacier Inventory**  
 69 **(RGI v7.0). Types of LTGs are shown in Table 1. Basemap hillshade is from Esri (World Hillshade)**

70 High Mountain Asia (HMA), encompassing the Tibetan Plateau and its surrounding ranges-  
 71 including the Himalayas, Karakoram, and Pamir Plateau, etc.-constitutes the most glacier-rich region in  
 72 the mid-latitudes (Figure 1). HMA lies between 26°-45°N and 67°-105°E. It has an average elevation of

73 approximately 4500 m (SRTM DEM). The region features a complex topography. This topography is  
74 characterized by higher elevations in the northwest and lower elevations in the southeast. It comprises a  
75 network of interwoven mountain ranges, valleys, and river systems. The dominant orographic orientation  
76 is east-west. The Tanggula Shan, located in the central part of the region, rise above 6000 m, while the  
77 Himalayas contain 15 peaks exceeding 8000 m, and most peaks on the northern plateau surpass 6500 m.  
78 North-south trending ranges are mainly distributed in the southeastern Tibetan Plateau and the Hengduan  
79 Shan, forming the geomorphological framework of the region and controlling the overall topographic  
80 configuration of the plateau.

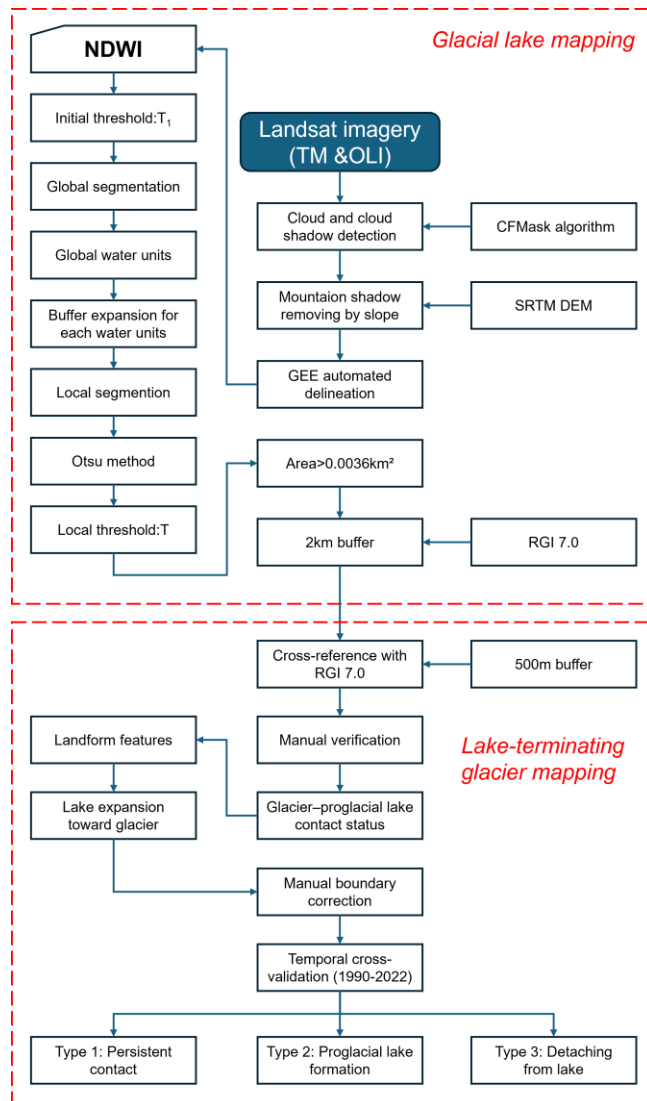
81 Climatically, HMA lies in the transition zone between the midlatitude westerlies and the Asian  
82 monsoon systems, leading to pronounced seasonal and spatial contrasts (Yao et al., 2012). In general,  
83 the southern and eastern sectors receive most precipitation during the summer monsoon, whereas the  
84 northern and western sectors are more strongly influenced by the westerlies, with overall drier conditions  
85 and a larger contribution from cold-season precipitation (Khanal et al., 2023). This pronounced  
86 hydroclimatic gradient produces highly heterogeneous pattern of glacier accumulation and ablation  
87 across the region. HMA is the headwater region for several major Asian rivers, including the Yellow  
88 River, Yangtze River, Yarlung Tsangpo, Indus, Ganges, Salween, Mekong, and Irrawaddy, and thus  
89 plays an important role in downstream hydrology and water resource. According to the Randolph Glacier  
90 Inventory (RGI 7.0), HMA contain 131761 modern glaciers with a total area of approximately  
91 99625.7km<sup>2</sup>, making it the most extensively glacierized region outside polar areas. The Karakoram hosts  
92 the largest number of glaciers, totalling 13988, and accounts for the largest share of glacier area at 29%.  
93 In contrast, the eastern Tibetan Plateau contains the fewest glaciers, with 819. The Eastern Tibetan  
94 Mountains represent the lowest glacier-area share, at 0.1%. Most glaciers in HMA are undergoing retreat  
95 (Brun et al., 2017; Hugonnet et al., 2021). However, slight mass gains have been observed in parts of the  
96 Karakoram and western Kunlun ranges (Gardelle et al., 2012; Kääb et al., 2015), though recent studies  
97 suggest this trend may be diminishing (Hugonnet et al., 2021). Glacial lakes are also widespread across  
98 HMA. Based on a recent manually interpreted inventory (Wang et al., 2020), 27205 and 30121 glacial  
99 lakes were mapped in 1990 and 2018, with total areas of  $1806.47 \pm 2.11$  km<sup>2</sup> and  $2080.12 \pm 2.28$  km<sup>2</sup>,  
100 respectively. This inventory includes the Altai and Sayan region, which is not part of our HMA definition.

101 The largest glacial lake areas were concentrated in the Altai and Sayan ( $335.42 \pm 0.88 \text{ km}^2$ , 16.1% of the  
102 total) and the eastern Himalaya ( $310.37 \pm 0.89 \text{ km}^2$ , 14.9%). In contrast, relatively small lake areas were  
103 found in the eastern Kunlun and Qilian Shan ( $38.85 \pm 0.29 \text{ km}^2$ , 1.9%) and the eastern Tien Shan ( $40.55$   
104  $\pm 0.32 \text{ km}^2$ , 2.0%). Over 1990–2018, glacial lakes across HMA experienced widespread areal expansion,  
105 with an average increase of 15.2%

### 106 **3 Data and methodology**

#### 107 **3.1 Extraction of proglacial lake outlines**

108 Before developing a comprehensive inventory of LTGs shown in [Fig. 1](#), we first generated a  
109 proglacial lake dataset using an automated delineation workflow within the Google Earth Engine (GEE)  
110 platform ([Figure 2](#)). We used Landsat imagery from the Thematic Mapper (TM) and Operational Land  
111 Imager (OLI) sensors, selected for their long-term record (since 1972), 30 m resolution, global coverage,  
112 and open access. All images were pre-processed in GEE, including radiometric, atmospheric, and  
113 geometric corrections. To minimize seasonal variability and the presence of snow and ice, we selected  
114 images acquired from July to November. Two-time windows were defined:  $1990 \pm 2$  years (historical)  
115 and  $2022 \pm 1$  year (recent). Due to limited image availability around 1990, imagery from 1993 to 1996  
116 was used to supplement data gaps. A 2 km buffer around each glacier was applied to focus on potential  
117 ice-contact proglacial lakes. Cloud contamination was reduced using the CFMask algorithm (Foga et al.,  
118 2017) to detect and mask clouds and shadows, followed by compositing cloud-free mosaics ([Figure 3a](#),  
119 [b](#)). In total, 4570 Landsat TM scenes were used for the 1990 period and 5493 OLI scenes for the 2020  
120 period ([Figure 3c, d](#)).



121

122 **Figure 2. Mapping workflow for lake-terminating glaciers and proglacial lakes**

123

124

125

126

127

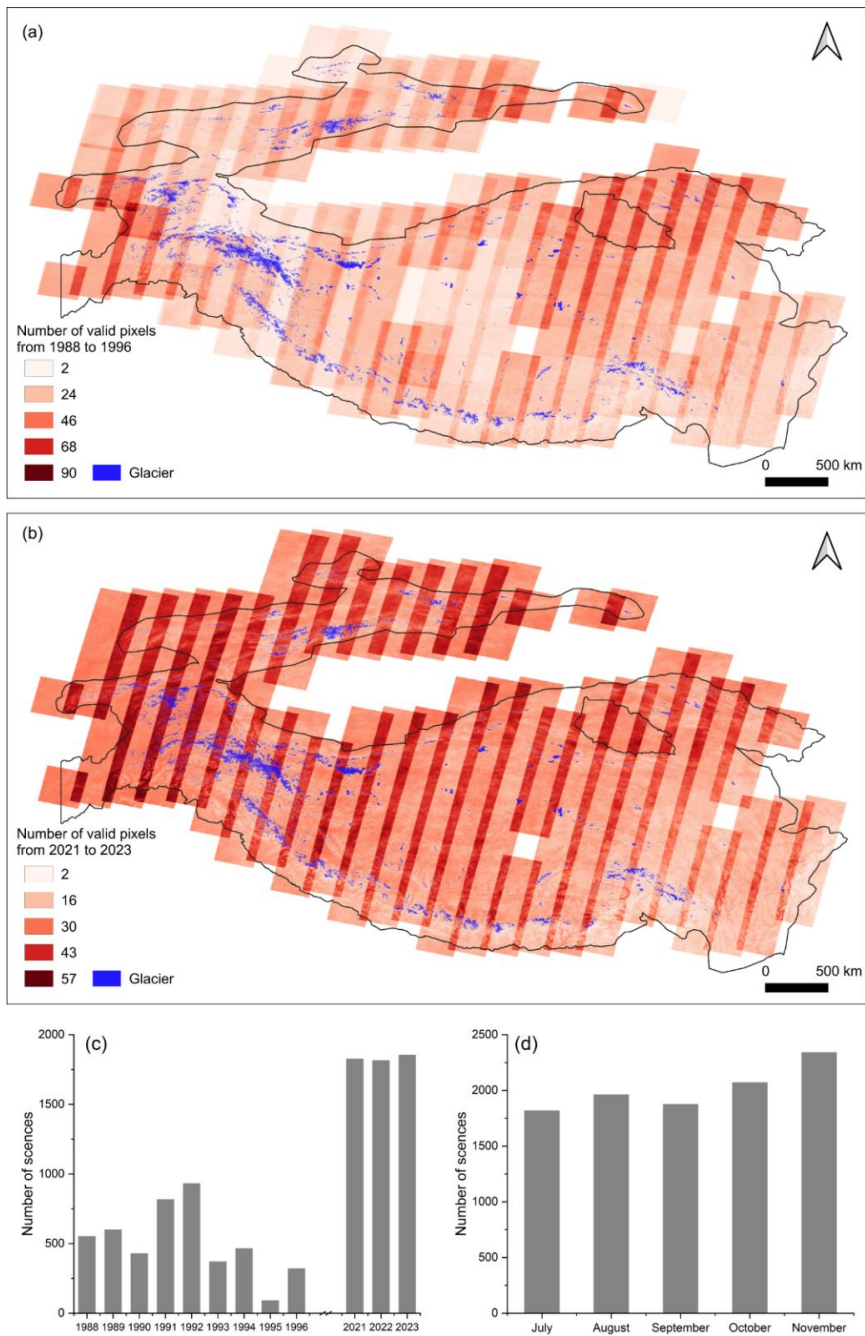
128

129

130

131

Glacial lake extents were delineated using an automated mapping algorithm based on hierarchical image segmentation and terrain analysis (Li and Sheng, 2012; Zhang et al., 2017). To reduce the influence of mountain shadows, pixels with slopes  $>20^\circ$  or shaded relief values  $<0.25$  were excluded (Zheng et al., 2021b). Previous studies applied varying minimum area thresholds for glacial lake identification:  $0.0054 \text{ km}^2$  (Wang et al., 2020),  $0.0081 \text{ km}^2$  (Chen et al., 2021),  $0.0036 \text{ km}^2$  (Luo et al., 2020), and  $0.01 \text{ km}^2$  (Li et al., 2020). Smaller thresholds can lead to greater uncertainties due to the limitations of pixel resolution (Salerno et al., 2012). To improve the accuracy of lake-terminating glacier identification, we adopted a minimum lake area threshold of  $0.0036 \text{ km}^2$  (equivalent to at least four pixels), following Luo et al. (2020).



132  
 133 **Figure 3. The number of usable pixels remaining in the study area after cloud removal during 1988–1996 (a)**  
 134 **and 2021–2023 (b). Temporal distribution of the number of images used, by year (c) and by month (d).**

135 **3.2 Mapping of LTGs**

136 In this study, LTGs are defined as glaciers that develop proglacial lakes along the direction of ice  
 137 flow and are in direct contact with these lakes. The proglacial lake dataset was cross-referenced with the  
 138 RGI 7.0 glacier inventory to identify LTGs. Results were refined through detailed visual inspection and  
 139 manual correction using multi-source data, including Landsat and PlanetScope imagery, online maps  
 140 (e.g., Google Earth, Esri basemap), and existing glacial lake datasets (Wang et al. 2020, Chen et al. 2021,

141 Zhang et al. 2023). The identification of glacier-lake contact followed a two-step procedure. (1)  
142 Preliminary screening: A 500 m buffer was applied to assess spatial intersections between glacier  
143 boundaries and proglacial lakes, identifying potentially connected glacier-lake pairs. (2) Manual  
144 verification: Different criteria were applied for different periods. For the year 2020, multi-source  
145 moderate-to-high resolution imagery (e.g., PlanetScope, Landsat, Google Earth, Esri basemaps) was used.  
146 Glacier-lake contact was confirmed when proglacial lakes overlapped with glacier terminus and  
147 exhibited diagnostic geomorphic features, such as terminal ice cliffs or transverse crevasses  
148 perpendicular to the flow direction. Due to limited data availability and the relatively coarse spatial  
149 resolution of Landsat imagery (30 m) in 1990, direct identification of LTGs for that year involved  
150 considerable uncertainty, particularly for small glaciers, where boundary errors increase with decreasing  
151 glacier area. To address this, a temporal cross-validation approach was employed. Glaciers with  
152 ambiguous contact in 1990 were classified as interacting if satellite imagery from 1990 to 2022 showed  
153 lake expansion toward the glacier terminus. Based on the temporal evolution of glacier-lake contact,  
154 LTGs were categorized into three types (Figure 4): (1) terminus persistent contacting with proglacial  
155 lake (Type 1); (2) terminus experiencing transition from supraglacial lake to proglacial lake (Type 2);  
156 and (3) terminus detaching from proglacial lake (Type 3).

Types	Characteristics			
Type 1	Persistent contact between glacier and lake from 1990 to 2022.  Case location: 94.51053E, 30.63100N			
Type 2	Transition from supraglacial lake to proglacial lake from 1990 to 2022.  Case location: 88.23816E, 27.81772N			
Type 3	Detachment of the proglacial lake from the parent glacier from 1990 to 2022.  Case location: 85.84583E, 28.20793N			

157

158 Figure 4 The classification system of glaciers is based on the dynamic changes in glacier–lake contact. The  
159 basemap is derived from Landsat imagery.

### 160 3.3 Uncertainty estimates

161 When interpreting glacial lake and glacier boundaries using remote sensing data, errors are  
162 inevitable even when manual visual delineation is applied. These errors are typically associated with  
163 various factors related to image quality, such as spatial resolution, cloud cover, mountain shadows, and  
164 subjective interpretation biases. Previous studies have reported that the area error in delineating glacier  
165 or glacial lake boundaries from remote sensing imagery is approximately  $\pm 0.5$  pixels, depending on the  
166 quality of the imagery. The uncertainty ( $\delta$ ) and relative error ( $E_l$ ) of glacial lake area was estimated using  
167 the equation (Hanshaw and Bookhagen, 2014):

$$168 \quad \delta = \frac{P}{G} \times \frac{G^2}{2} \times 0.6872 \quad (1)$$

$$169 \quad E_l = \frac{\delta}{A} \times 100\% \quad (2)$$

170 where  $P$  is the perimeter of the glacial lake, and  $A$  is the glacial lake area.

171 The uncertainty ( $\lambda$ ) and relative error ( $E_g$ ) in glacier area was estimated to using the equation (Bolch  
172 et al., 2010):

173 
$$\lambda = N \times \frac{G^2}{2} \quad (3)$$

174 
$$E_g = \frac{\lambda}{S} \times 100\% \quad (4)$$

175 where  $N$  is the total count of pixels along the outline of ice coverage,  $G$  is the spatial resolution of the  
176 images used, and  $S$  is the glacier area.

### 177 **3.4 Attributes of inventory data**

178 In this inventory, 9 attribute fields (Table 1) were recorded for the LTG, including a unique identifier,  
179 type, associated mountain range, area, mapping uncertainty, location (longitude and latitude), RGI7 ID,  
180 and feature code. Similarly, the proglacial lake inventory contains 9 attribute fields (Table 2), including  
181 a unique identifier, associated mountain range, type, mapping uncertainty, location (longitude and  
182 latitude), feature code, and a flag indicating whether the lake has disappeared. Both LTG and proglacial  
183 lake datasets include data for two time periods: 1990 and 2022, with identical attributes for both periods.  
184 The unique identifier is an automatically generated sequential integer, while the feature code follows the  
185 formats GmmmmmmEnnnnnN (Feature\_ID) for glaciers and GLmmmmmmEnnnnnN (Featruue\_ID) for  
186 lakes, where G denotes glacier, GL denotes glacier lake, m and n represent the longitude and latitude  
187 multiplied by 1000, respectively, and E and N indicate east longitude and north latitude. Identical LTGs  
188 and proglacial lakes share the same feature code (Feature\_ID) to facilitate data linkage. Area and  
189 perimeter are calculated automatically from the feature geometry. The type of classification follows the  
190 criteria described in Section 3.2. Each feature's associated mountain range is determined by overlaying  
191 with mountain range boundaries, and mapping uncertainty is estimated according to Sect. 3.3.

192

193

194

195

196

197

198

199

200 **Table 1. Attributes of the glacier dataset**

<b>Filed name</b>	<b>Type</b>	<b>Description</b>
UID	Object ID	Unique code (Number)
Type	String	The classification of glaciers based on the relationship of interaction between glaciers and glacial lakes (Figure 4)
Mountain	String	Mountain name where the glaciers is in
Area	Double	Area of glacier coverage(km <sup>2</sup> )
Error	Double	Area uncertainty of glacier mapping(km <sup>2</sup> )
Latitude	String	Latitude of the centroid of glacier
Longitude	String	Longitude of the centroid of glacier
rgi_id	String	RGI 7.0 id
Feature_ID	String	GmmmmmmEnnnnnN

201

202 **Table 2. Attributes of the proglacial lake dataset**

<b>Filed name</b>	<b>Type</b>	<b>Description</b>
UID	Object ID	Unique code (Number)
Type	String	The classification of glacial lakes based on the relationship of interaction between glaciers and glacial lakes (Figure 4)
Mountain	String	Mountain name where the glacial lake is in
Area	Double	Area of glacial lake coverage (km <sup>2</sup> )
Error	Double	Area uncertainty of glacial lake mapping (km <sup>2</sup> )
Latitude	String	Latitude of the centroid of glacier

---

Longitude	String	Longitude of the centroid of glacier
Disappear	String	Whether the proglacial lake disappeared in 2022 (Y)
Feature_ID	String	GLmmmmmmEnnnnnN

---

203

204 **4 Results**

205 **4.1 Spatial distribution of LTGs and proglacial lakes**

206 Based on the changes in glacier-proglacial lake contact relationships from 1990 to 2022, glaciers  
 207 were classified into three types (Figure 4). Among them, Type 1 and Type 2 glaciers remained in contact  
 208 with proglacial lakes in 2022 and are therefore defined as LTGs. In contrast, Type 3 glaciers had become  
 209 disconnected from proglacial lakes by 2022. Accordingly, only Type 1 and Type 2 glaciers were included  
 210 when analyzing the distribution and extent of LTGs in 2022. In 2022, a total of 1740 LTGs were  
 211 identified, with a combined area of  $5082.08 \pm 13.15 \text{ km}^2$ . Concurrently, 1768 proglacial lakes were  
 212 detected, with a total area of  $262.10 \pm 0.89 \text{ km}^2$ . The discrepancy between glacier and lake counts stems  
 213 from multi-lake associations per glacier and multi-glacier lakes were associated with two glaciers, and  
 214 two lakes were in contact with three glaciers. The distribution of LTGs in HMA shows marked  
 215 heterogeneity (Figure 5). Predominantly concentrated along the southern margin, including the  
 216 Himalayas, Nyainqentanglha, Gangdise Mountains, and Hindu Kush, these glaciers total 994,  
 217 representing 57.13% of the study population (Figure 5b, Table S1). The Central Himalaya hosts the  
 218 highest number, with 232 glaciers (Table S1), while the Nyainqentanglha accounts for the largest total  
 219 glacier area ( $1001.05 \pm 3.32 \text{ km}^2$ , Figure 5c). Glaciers were classified into nine size categories, ranging  
 220 from  $<0.05 \text{ km}^2$  to  $>100 \text{ km}^2$  (Table S2). Among these, 1095 glaciers (62.93%) are smaller than  $1 \text{ km}^2$ ,  
 221 covering  $399.05 \pm 1.07 \text{ km}^2$  (7.85% of the total area), while 93 glaciers (5.35%) exceed  $10 \text{ km}^2$ , covering  
 222  $2964.68 \pm 4.85 \text{ km}^2$  (58.34%). Only three glaciers exceed  $100 \text{ km}^2$ , spanning  $785.42 \pm 10.96 \text{ km}^2$ . LTGs  
 223 in HMA span elevations from 2735 to 8016 m, with a mean elevation of 5074 m (Figure 6). They are  
 224 primarily concentrated between 5000 and 6000 m, where their combined area reaches  $3030.2 \pm 5.72 \text{ km}^2$   
 225 (59.52% of the total glacier area). Regional variations in elevation distribution are evident (Figure 6). In

226 the Central Himalaya, Eastern Himalaya, Gangdise Mountains, Tibetan Interior Mountains, and Western  
227 Kunlun Shan, glacier area peaks occur around 6000 meters.

228 Proglacial lakes in HMA are predominantly concentrated along the southern margin, with 1010  
229 lakes (57.09%) in the Himalayas, Nyainqentanglha, Gangdise Mountains, and Hindu Kush (Table S3).  
230 The Central Himalayas host the most lakes (240), with the largest total area ( $86.91 \pm 0.54 \text{ km}^2$ , Figure 5  
231 e). Proglacial lakes were grouped into five size categories ( $<0.05$  to  $>1 \text{ km}^2$ , Table S4). Lakes smaller  
232 than  $0.1 \text{ km}^2$  are the most abundant, totaling 1384 (78.28%) and covering a combined area of  $47.12 \pm$   
233  $0.30 \text{ km}^2$ . Proglacial lakes in HMA span elevations from 2684 to 6012 m, with most concentrated  
234 between 5000 and 5700 m, where 748 lakes (42.34%) cover  $106.46 \pm 0.59 \text{ km}^2$ . Regional variations in  
235 elevation distribution are evident (Figure 7). Gangdise Mountains and Western Kunlun Shan, proglacial  
236 lake numbers and areas peak around 5700 m. Conversely, in the Hindu Kush, Nyainqentanglha, Tanggula  
237 Shan, and Western Kunlun Shan, peak lake areas occur at lower elevations than peak lake numbers  
238 (Figure 7).

239 Significant variations exist in the number and area distributions among glacier types in HMA. From  
240 1990 to 2022, Type 2 glaciers, those forming new proglacial lakes, were the most numerous (1073, Table  
241 S1), dominating in all regions except Altun Shan/Eastern Kunlun Shan, Qilian Shan, and Tanggula Shan.  
242 Conversely, Type 1 glaciers have the largest total area ( $3454.59 \pm 12.43 \text{ km}^2$ ), concentrated primarily in  
243 the Himalayas, Nyainqentanglha, Central Tien Shan, Qilian Shan, Tanggula Shan, and Western Kunlun  
244 Shan (Table S1). The Central Himalaya host the most glaciers across all types: 94 Type 1 ( $552.77 \pm 2.71$   
245  $\text{km}^2$ ), 138 Type 2 ( $244.80 \pm 1.56 \text{ km}^2$ ), and 84 Type 3 ( $202.67 \pm 1.11 \text{ km}^2$ ). All glacier types show  
246 consistent area peaks between 5000 and 6000 m, with similar patterns across subregions (Figure 6). In  
247 2022, Type 2 proglacial lakes were the most numerous in HMA (1123, Table S3), dominating in number  
248 across all regions except Altun Shan/Eastern Kunlun Shan, Qilian Shan, Karakoram, and Western  
249 Kunlun Shan. Conversely, Type 1 lakes had the largest total area ( $207.18 \pm 0.82 \text{ km}^2$ ) and accounted for  
250 the largest share of total area in all regions except the Western Pamir, Hengduan Shan, Dzhungarsky  
251 Alatau, and Eastern Tibetan Mountains. The central Himalaya hosted the greatest abundance of all three  
252 lake types, with 91 Type 1 ( $76.89 \pm 0.51 \text{ km}^2$ ), 149 Type 2, and 80 Type 3 ( $15.70 \pm 0.21 \text{ km}^2$ ) lakes. The  
253 Eastern Himalaya had the largest Type 2 lake area ( $10.73 \pm 0.03 \text{ km}^2$ , Table S3). In HMA, the elevation

254 distribution of proglacial lake types is generally consistent, with peak numbers between 5000 and 5700  
255 m and peak areas between 4700 and 5400 m (Figure 7). However, regional variations are observed in  
256 the elevation distribution of lake numbers for different lake types. Specifically, in the Nyainqentanglha  
257 region, Type 2 proglacial lakes exhibit a higher peak number range, between 5200 and 5400 m.  
258 Regarding area-elevation patterns, certain subregions display lower peak elevations, encompassing Type  
259 2 lakes in the Eastern Himalaya and Northern Tibetan Mountains, and Type 1 lakes in the Eastern Pamirs,  
260 Hindu Kush, Nyainqentanglha, and Tanggula Shan (Figure 6).

#### 261 4.2 Temporal changes in LTGs and proglacial lakes

262 From 1990 to 2022, glacier size has been continuously shrinking (Figure 5d). The total area of all  
263 glacier types decreased by approximately  $324.43 \pm 19.22$  km<sup>2</sup>, with Type 1 glaciers experiencing the  
264 largest absolute loss of  $137.46 \pm 17.62$  km<sup>2</sup>, accounting for 42.37% of the total reduction (Table S5). The  
265 Central Himalay showed the most pronounced absolute area loss, with a decrease of  $74.46 \pm 3.46$  km<sup>2</sup>,  
266 while the Hengduan Shan exhibited the highest relative shrinkage at 16.42%. The Central Himalaya also  
267 recorded the largest absolute losses for all three glacier types, with reductions of  $37.20 \pm 3.91$  km<sup>2</sup> for  
268 Type 1,  $20.13 \pm 2.26$  km<sup>2</sup> for Type 2, and  $17.13 \pm 1.62$  km<sup>2</sup> for Type 3 glaciers. In contrast, the Hengduan  
269 Shan had the highest relative losses for all three types, at 25.34%, 13.95%, and 17.37%, respectively  
270 (Table S5).

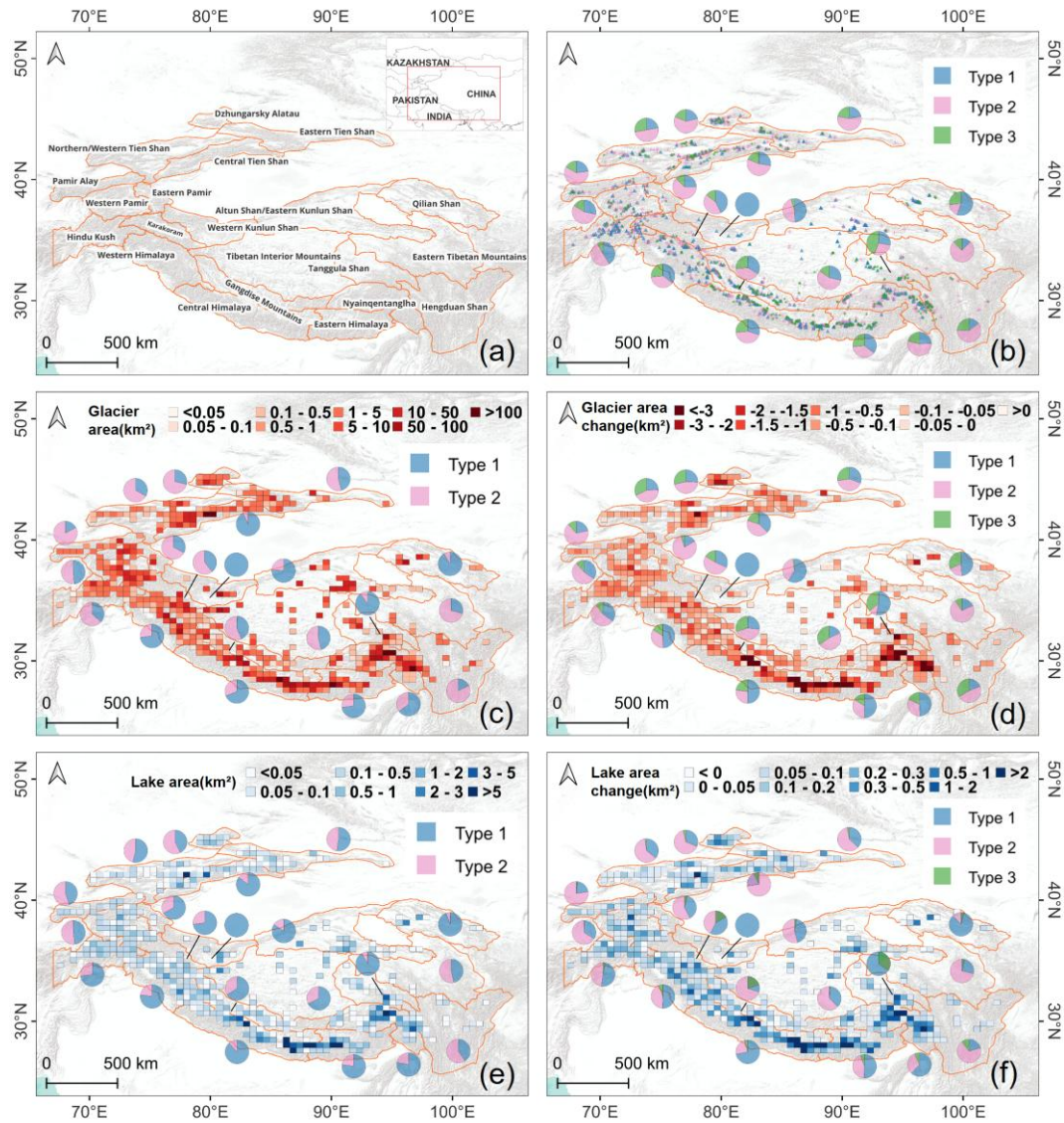
271 Small glaciers (<0.5 km<sup>2</sup>) exhibited a significant increase in number, particularly those smaller than  
272 0.05 km<sup>2</sup>, which grew by 51 in count with a total area increase of  $1.68 \pm 0.08$  km<sup>2</sup> (Table S6). In contrast,  
273 glaciers in the 0.5–50 km<sup>2</sup> range showed a declining trend in number. Among them, glaciers sized 0.5–1  
274 km<sup>2</sup> experienced the largest numerical decrease (–57) and the greatest relative area loss (–13.56%), while  
275 those in the 1–5 km<sup>2</sup> range incurred the most substantial absolute area reduction, losing  $97.17 \pm 3.5$  km<sup>2</sup>  
276 (Table S6).

277 Among the different glacier types, Type 1 glaciers experienced the greatest absolute area loss,  
278 decreasing by  $137.46 \pm 17.62$  km<sup>2</sup> (Table S5). However, their relative area reduction of 3.83% was the  
279 smallest among the three types. By size class (Table S6), Type 1 glaciers showed the largest loss ( $63.39$   
280  $\pm 6.38$  km<sup>2</sup>) in the 10–50 km<sup>2</sup> range; Type 2 glaciers experienced the greatest reduction ( $52.52 \pm 2.21$   
281 km<sup>2</sup>) in the 1–5 km<sup>2</sup> range. Type 3 glaciers showed the most significant loss ( $27.51 \pm 1.57$  km<sup>2</sup>) in the 5–

282 10 km<sup>2</sup> range. For all three types, the 0.5–1 km<sup>2</sup> size class exhibited the highest relative area reduction,  
283 at 9.06%, 15.37%, and 15.15%, respectively.

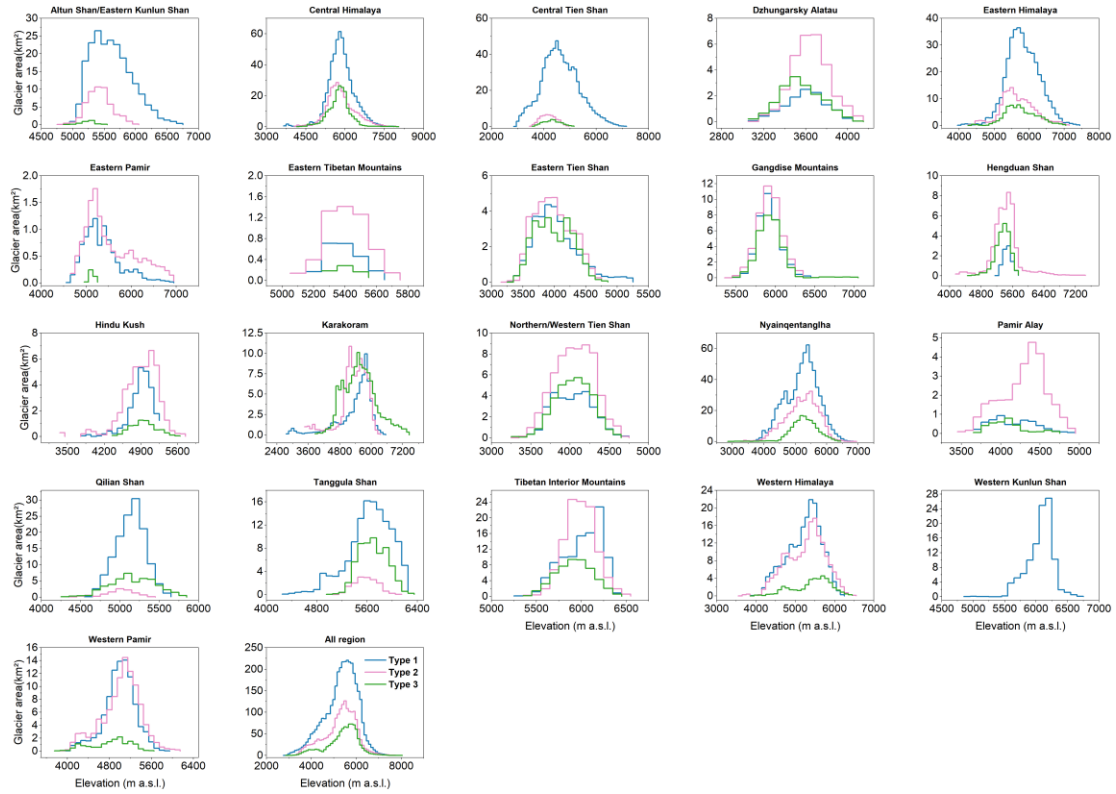
284 Between 1990 and 2022, the total area of proglacial lakes increased by  $138.19 \pm 1.18$  km<sup>2</sup>,  
285 representing a 62.09% expansion (Figure 5f and Table S2). The Central Himalaya experienced the most  
286 significant absolute growth, with an increase of  $42.32 \pm 0.72$  km<sup>2</sup> (70.19%), while the Western Pamirs  
287 recorded the fastest relative growth, surging by 210.24%. The Central Himalaya also saw the largest area  
288 increases across all three glacier types, with growth of  $30.42 \pm 0.64$  km<sup>2</sup> for Type 1 lakes,  $10.02 \pm 0.16$   
289 km<sup>2</sup> for Type 2, and  $1.88 \pm 0.29$  km<sup>2</sup> for Type 3. Regionally, the Dzhungarsky Alatau had the highest  
290 proportional increase in Type 1 lake area at 176.38%, whereas the Eastern Himalaya recorded the largest  
291 proportional growth for Type 3 lakes at 29.48% (Table S7).

292 During the study period, 1123 new proglacial lakes formed, while 25 lakes disappeared. The number  
293 of small proglacial lakes (<0.5 km<sup>2</sup>) increased significantly, especially those smaller than 0.05 km<sup>2</sup>,  
294 which increased by 702 and accounted for 64.11% of the total increase in lake numbers (Table S8). Lakes  
295 larger than 1 km<sup>2</sup> contributed the largest increase in area ( $60.44 \pm 0.81$  km<sup>2</sup>), accounting for 43.74% of  
296 the total area growth. Moreover, lakes smaller than 0.05 km<sup>2</sup> had the highest proportional area growth at  
297 114.49%. Type 1 proglacial lakes exhibited the most significant area growth, reaching  $79.36 \pm 1.02$  km<sup>2</sup>,  
298 with a growth rate of 62.09%. Among size categories, the number of Type 1 lakes increased most in the  
299 0.05–0.1 km<sup>2</sup> range, with 49 new lakes added, while lakes larger than 1 km<sup>2</sup> showed the greatest area  
300 increase at  $52.07 \pm 0.79$  km<sup>2</sup> and the highest proportional growth at 85.19%.



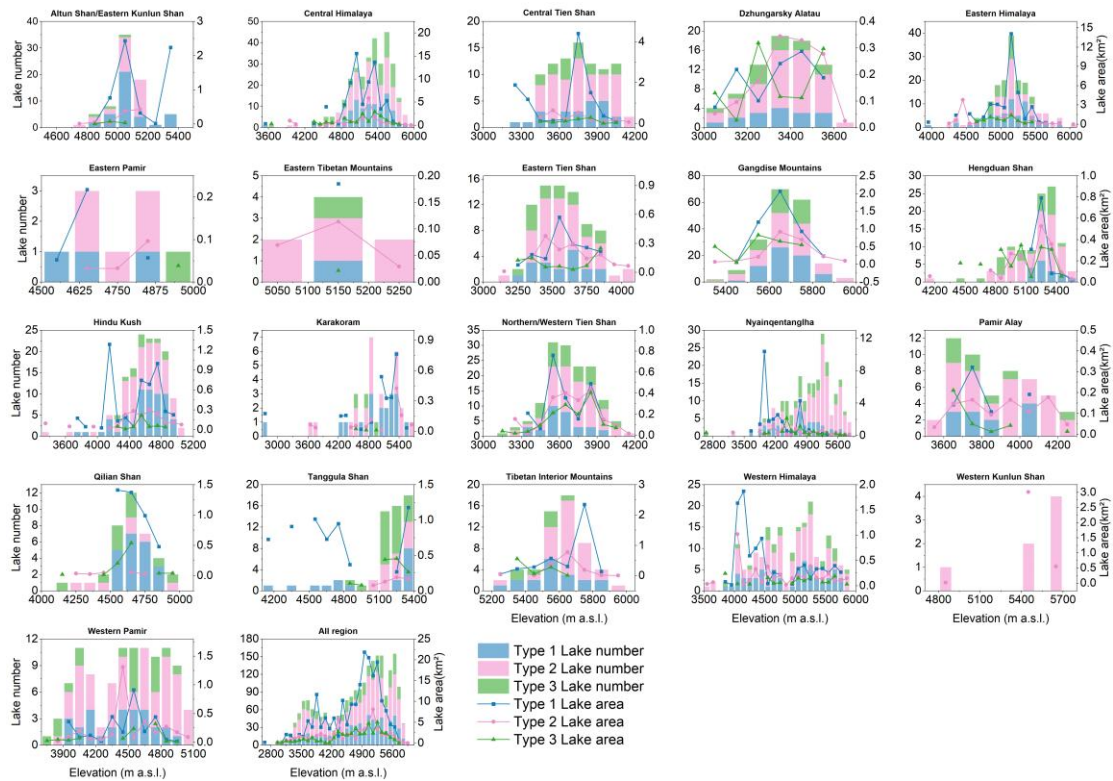
301  
 302 **Figure 5. (a) Geographic extent of the mountain ranges in HMA. (b) Distribution of the three types of LTGs**  
 303 **in 2022 and their numerical proportions across mountain regions. (c) Size distribution (Types 1 and 2) in 2022**  
 304 **and their area proportions. (d) Area changes of the three types of glaciers from 1990 to 2022 and their area-**  
 305 **change proportions across mountain regions. (e) Area distribution of proglacial lakes (associated with Types**  
 306 **1 and 2 glaciers) in 2022 and their area proportions across mountain regions. (f) Area changes of the three**  
 307 **types of proglacial lakes from 1990 to 2022 and their area-change proportions across mountain regions.**  
 308 **Basemap hillshade is from Esri (World Hillshade).**

309



310

311 **Figure 6. Area-Elevation distribution of LTGs across subregions, showing glacier area within 100 m elevation**  
 312 **bins.**



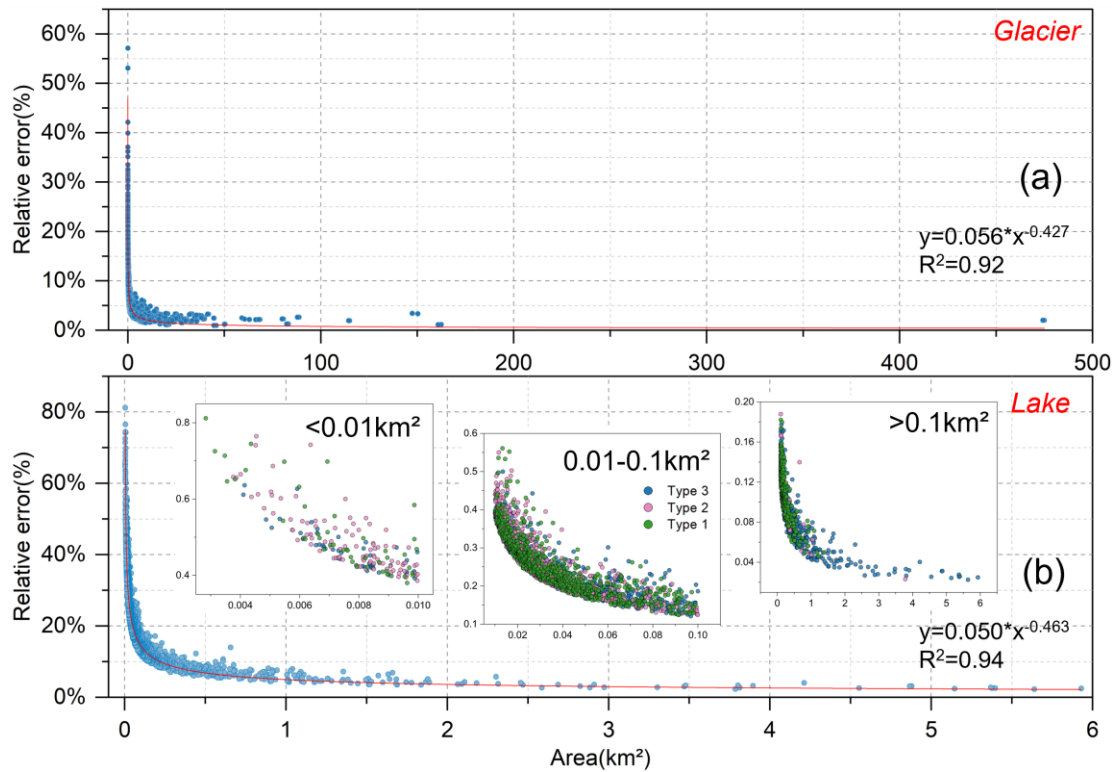
313

314 **Figure 7. Distribution of proglacial lake numbers and areas across elevation ranges in each subregion. The**  
 315 **number and area of proglacial lakes are presented within 100 m elevation bins for each subregion.**

## 316 5 Discussion

### 317 5.1 Assessment of accuracy and errors

318 The uncertainty estimates indicate that as the glacier or lake area increases, the relative error of  
319 individual features decreases. In the study area, the total absolute area error for glaciers in 1990 and 2022  
320 were  $\pm 13.65 \text{ km}^2$  and  $\pm 13.53 \text{ km}^2$ , respectively, with average relative errors of  $\pm 7.24\%$  and  $\pm$   
321  $8.12\%$ . The relative error of glacier area shows a significant power-law relationship with the glacier size  
322 ( $y = 0.056 \times x^{-0.427}$ ,  $R^2 = 0.92$ , [Figure 8a](#)). Additionally, the total absolute area error for proglacial  
323 lakes in 1990 and 2022 were  $\pm 0.69 \text{ km}^2$  and  $\pm 0.96 \text{ km}^2$ , respectively, with average relative errors of  
324  $\pm 21.99\%$  and  $\pm 23.69\%$ , following a similar significant power-law relationship ( $y = 0.050 \times x^{-0.463}$ ,  
325  $R^2 = 0.94$ , [Figure 8b](#)). We found that the maximum relative error for proglacial lakes exceeds 80%. We  
326 therefore stratified relative error statistics by lake area bins and glacier types. The largest errors are  
327 primarily associated with lakes smaller than  $0.01 \text{ km}^2$ , which have a mean relative error of 49%. Within  
328 this size class, Type 2 proglacial lakes are most prevalent, accounting for 52% of all lakes  $<0.01 \text{ km}^2$ . To  
329 better constrain the impact of these small lakes on overall dataset accuracy, we visually verified them  
330 using higher resolution remote sensing imagery (PlanetScope, Esri basemaps, and Google imagery),  
331 thereby reducing misidentification arising from limited spatial resolution.



332

333 **Figure 8. Estimation of relative errors for glaciers and proglacial lakes in the study area. (a) Glaciers (b)**  
 334 **Proglacial lakes. We also divided the proglacial lakes into three area intervals and quantified the relative**  
 335 **errors for different types.**

336 **5.2 Comparison and limitations**

337 Publicly available data on LTGs and their proglacial lakes in HMA remain scarce, with recent  
 338 datasets primarily focusing on glacial lakes. Consequently, this study selected two glacial lake datasets  
 339 that partially overlap in time with our research and include proglacial lakes for comparison (Table 3).  
 340 The results indicate that, within the same study area, our data closely align with those of Zhang et al.  
 341 (2023). In 1990, the overlap rate of proglacial lakes between the dataset of Zhang et al. (2023) and ours  
 342 exceeded 90%, while in 2020/2022, the overlap rate was 79%. In contrast, significant discrepancies were  
 343 observed with the dataset of Chen et al. (2021). For the period 2017/2022, the dataset of Chen et al. (2021)  
 344 identified 7850 proglacial lakes, whereas our study identified only 1768, with an overlap rate of 67.82%.  
 345 To further clarify the causes of these discrepancies, we selected a representative subregion in the central  
 346 Himalaya as a sample area for cross-validation (Fig. S1). Our dataset indicates that 45 proglacial lakes  
 347 were present in this area in 2022. In contrast, Chen et al. (2021) reported 335 glacial lakes in 2017, of  
 348 which only 29 (64% of our proglacial lakes) overlap with our inventory. Zhang et al. (2023) reported 38  
 349 proglacial lakes in 2020, with 30 (67%) overlapping with our results. Chen et al. (2021) likely used a

350 more permissive definition when screening lakes in front of glacier termini, effectively including many  
351 water bodies that are not in direct contact with glacier. We apply strict criterion (Sect. 3.2) and define  
352 proglacial lakes as those that are in contact with glacier ice and situated at the downstream end along the  
353 glacier flow direction. Part of the mismatch may also arise from differences in lake-type labeling during  
354 transitional stages. Several water bodies that we classify as proglacial lakes were labeled as supraglacial  
355 lakes by Chen et al. (2021) and Zhang et al. (2023). In addition, some supraglacial ponds are currently  
356 merging and evolving into a single, unified proglacial lake, and we classify lakes with a high degree of  
357 transition as proglacial lakes. Differences in the minimum mapping area threshold further amplify the  
358 mismatch. Our inventory and Zhang et al. (2023) uses 0.0036 km<sup>2</sup>, whereas Chen et al. (2021) used  
359 0.0081 km<sup>2</sup>, which affects the inclusion of small lakes and therefore the total lake count. Finally, we  
360 corrected omissions in earlier inventories where applicable, and additional factors, such as image quality,  
361 acquisition dates, and vectorization workflows, may also contribute to the observed discrepancies.

362 A global inventory of LTGs was released in 2025 (Steiner et al., 2025). This dataset was derived  
363 from the RGI7 glacier outlines, primarily using Landsat 5 and 7 TM/ETM+ imagery (ca. 1998–2002),  
364 supplemented by ASTER data in some high-latitude regions (for a small portion of the Canadian Arctic  
365 and Greenland Periphery). Existing regional proglacial lake inventories (when close to 2000) were also  
366 incorporated, and the identification of LTGs was conducted through manual interpretation and expert  
367 cross-validation. Based on the degree of glacier–lake contact, glaciers were classified into three types  
368 (Level 1: glacier–lake contact exceeds 50% of the terminus perimeter. Level 2 : glacier–lake contact  
369 ranges from 10% to 50% of the terminus perimeter. Level 3: glacier–lake contact is less than 10% of the  
370 terminus perimeter.). In HMA, a total of 1912 LTGs were identified. Although the glacier termini in this  
371 dataset were delineated for 2000 ± 2, the overlap with our 2022 dataset is 50%. Specifically, our dataset  
372 shows an overlap rate of 63% with level 1 glaciers, 43% with level 2 glaciers, and 19% with level 3  
373 glaciers. The differences in results can be attributed to two primary factors. First, temporal differences.  
374 The reference dataset is mainly based on imagery from around the year 2000, whereas our dataset relies  
375 on imagery from around 2022. Given that glacier–lake contact relationships are inherently unstable (Luo  
376 et al., 2025), the emergence of newly formed proglacial lakes and glaciers that no longer maintain contact  
377 with proglacial lakes during this period may have significantly influenced the statistical outcomes.

378 Second, methodological differences. Although both studies adopt a broadly similar semi-automatic  
379 approach to screening glaciers based on lake data, the specific implementations differ. The reference  
380 dataset utilizes existing open-access lake inventories (Chen et al., 2021; Wang et al., 2020), while our  
381 lake dataset was extracted by ourselves, with different lake area thresholds applied (0.0054 km<sup>2</sup> and 0.0081  
382 km<sup>2</sup> in the reference dataset versus 0.0036 km<sup>2</sup> in our study). Such differences may contribute to  
383 discrepancies in the results. Moreover, the criteria for identifying lake-terminating glaciers also diverge.  
384 The reference dataset classifies glaciers according to the proportion of lake contact relative to the glacier  
385 terminus perimeter, whereas our study emphasizes geomorphological features (e.g., ice cliffs, crevasses)  
386 and the expansion trend of proglacial lakes, i.e., whether lakes continue to expand toward the glacier.  
387 Due to these differences in classification standards, our dataset may not include some of the level 2 and  
388 level 3 glaciers identified in the reference dataset, which likely explains the lower overlap rates with  
389 these categories.

390 Although this study employed standardized criteria for the qualitative identification of LTGs and  
391 their proglacial lakes, subjective factors remain challenging to eliminate entirely during remote sensing  
392 imagery analysis. Differences in how analysts interpret imagery, apply calibration standards, and process  
393 data quality directly impact the results. While measures such as independent labeling and cross-validation  
394 by multiple analysts can reduce subjective bias, uncertainties stemming from variations in individual  
395 experience, judgment criteria, and image quality remain difficult to fully resolve. Consequently, further  
396 quantification of identification criteria is of paramount importance. In the future, more refined technical  
397 approaches can optimize the identification of glacier-lake contact lines, leveraging high-resolution  
398 imagery and automated analysis tools to enhance accuracy. Additionally, quantifying the depth of  
399 glaciers within lakes will provide more precise data support. These quantitative standards not only  
400 effectively minimize human-induced variability but also significantly improve the precision of glacier-  
401 lake contact relationship assessments, laying a more reliable data foundation for subsequent studies of  
402 glacier dynamics.

403

404 **Table 3. Comparisons of glacial lake mapping in this study with previous studies for the similar extended**  
 405 **region.**

Year (previous/this study)	Region	Area threshold (km <sup>2</sup> )	Source	Count (Area/km <sup>2</sup> )	Count (Area/km <sup>2</sup> )	Overlap
				Previous studies	This study	count
1990/1990	Greater	0.0036	(Zhang et al.,	651(129.76±0.89)	645(122.08±0.59)	615(95.35%)
2020/2022	Himalaya		2023)	1115(192.42±1.23)	1029 (199.83±0.79)	841(79.11%)
2017/2022	HMA	0.0081	(Chen et al., 2021)	7850(684.62±10.06)	1768(262.03±0.89)	1199(67.82%)

406 **5.3 Drivers of changes in lake-terminating glaciers and associated disaster risks**

407 Climate warming is a primary driver of both the number and size of proglacial lakes, which in turn  
 408 has contributed to the increasing prevalence of lake-terminating glaciers (LTGs). Glaciers across High  
 409 Mountain Asia (HMA) have experienced widespread retreat during the 21st century (Brun et al., 2017;  
 410 Hugonnet et al., 2021), with the most significant mass losses occurring in the Nyainqentanglha region  
 411 ( $-0.62 \pm 0.23$  m w.e. a<sup>-1</sup>, locally reaching  $-0.80 \pm 0.25$  m w.e. a<sup>-1</sup>). Moderate mass losses are observed  
 412 in the central Himalaya, with rates of  $-0.42 \pm 0.20$  m w.e. a<sup>-1</sup> in Bhutan and  $-0.33 \pm 0.20$  m w.e. a<sup>-1</sup> in  
 413 eastern Nepal. Consequently, the Himalayan–southeastern Tibetan Plateau has emerged as a hotspot of  
 414 glacier wastage. Glacier retreat provides both the material supply and geomorphic setting for proglacial  
 415 lake development, fostering a high concentration of LTGs in this region. LTGs in the Himalayan–  
 416 southeastern Tibetan Plateau account for 61% of the total number of LTGs in HMA and 55% of newly  
 417 formed LTGs.

418 However, the formation of proglacial lakes is not solely driven by climate forcing; it also amplifies  
 419 the nonlinear response of glaciers to climate change. Proglacial lakes are closely linked to enhanced  
 420 glacier mass loss, primarily through processes such as subaqueous melting (Zhang et al., 2023),  
 421 accelerated ice flow (Pronk et al., 2021), and the potential risk of glacial lake outburst floods (Zheng et  
 422 al., 2021b). As glacial lakes expand, the increasing water depth at glacier termini further elevates the  
 423 uncertainty surrounding calving, as greater water depths are generally thought to accelerate terminus

424 collapse (Minowa et al., 2023). Incorporating glacier morphological variables (e.g., supraglacial debris  
425 cover, slope, elevation) into the analysis is, therefore, essential for understanding the role of proglacial  
426 lakes in influencing glacier mass balance. Monitoring of Bridge Glacier by Chernos et al. (2016) revealed  
427 that calving at the glacier terminus has consistently remained a secondary contributor to ablation. While  
428 calving accounted for up to 49% of ablation in some individual years, its multi-year average contribution  
429 was only 10–25%. Rapid retreat has been strongly associated with increasing water depth, but such high  
430 calving rates are typically transient and tend to decrease as glacier termini recede into shallower waters.  
431 Our results further demonstrate that glacier-lake contact relationships are inherently unstable. Between  
432 1990 and 2022, 41% of glaciers that were previously in contact with proglacial lakes lost this connection.  
433 This rapid change underscores the episodic and unstable nature of the influence of proglacial lakes on  
434 glacier evolution. Therefore, projections of glacier mass loss should consider not only climatic factors  
435 but also the evolving glacier-lake contact relationships and their heterogeneous impacts on glacier  
436 dynamics.

437       The risk of glacial lake outburst floods (GLOFs) in the High Mountain Asia (HMA) region is  
438 increasing under the backdrop of climate warming, particularly in the Himalaya (Zheng et al., 2021b).  
439 Our study finds that the total area of proglacial lake expansion in the southeastern Tibetan Plateau and  
440 eastern Himalayas accounts for 78% of the total glacial lake expansion in the HMA. As glaciers retreat,  
441 proglacial lakes in contact with them expose their basins. This significantly increases their potential for  
442 expansion compared to other types of glacial lakes, making them a higher-risk disaster source. Over the  
443 past three decades, 188 GLOF events have been recorded in the HMA (Shrestha et al., 2023), of which  
444 55 events (29%) occurred in glacier-proglacial lake systems. The main triggers of these floods include  
445 ice avalanches (Sherpa et al., 2025) and slope instability caused by rapid glacier retreat, leading to  
446 landslides into the lakes (Zheng et al., 2021a). Due to the continuous impact of climate warming, the  
447 interactions between glaciers and proglacial lakes may become increasingly complex in the coming  
448 decades. The number and size of glacial lakes may further increase, and the relationships between  
449 glaciers and proglacial lakes may undergo significant changes. As a result, traditional climate-based  
450 disaster risk models may not fully capture these complex, nonlinear interactions, especially those  
451 involving glacial lake expansion and glacier retreat. To effectively address these challenges, future

452 disaster risk management strategies must be more comprehensive and forward-looking. This should  
453 include strengthening monitoring and early warning systems for GLOFs, incorporating the evolution of  
454 glacier-lake contact relationships, and considering glacier morphological characteristics to improve  
455 prediction capabilities.

## 456 **6 Conclusions**

457 Using Landsat imagery, we applied a semi-automated mapping approach in Google Earth Engine  
458 (GEE) to inventory proglacial lakes across High Mountain Asia (HMA) in the 1990s and 2020s, and  
459 compiled the first region-wide dataset of LTGs and their proglacial lakes. In 2022, HMA contained 1740  
460 LTGs ( $5082.08 \pm 13.15 \text{ km}^2$ ), of which 667 glaciers ( $3454.59 \pm 12.43 \text{ km}^2$ ) maintained lake contact since  
461 1990, and 1073 glaciers ( $1,627.49 \pm 4.30 \text{ km}^2$ ) developed new proglacial lakes. These glaciers were  
462 mainly distributed between 2735 and 8016 m a.s.l. Additionally, 468 glaciers ( $960.13 \pm 3.18 \text{ km}^2$ ) lost  
463 lake contact during the period.

464 A total of 1768 proglacial lakes ( $262.10 \pm 0.89 \text{ km}^2$ ) were connected to glaciers in 2022, including  
465 645 lakes ( $207.18 \pm 0.82 \text{ km}^2$ ) with continuous glacier contact and 1123 newly formed lakes ( $54.85 \pm$   
466  $0.35 \text{ km}^2$ ). Lakes were mainly distributed between 2684 and 6012 m a.s.l. Meanwhile, 485 lakes ( $45.31$   
467  $\pm 0.34 \text{ km}^2$ ) lost glacier contact, with 25 disappearing entirely. From 1990 to 2022, LTGs retreated by  
468  $324.43 \pm 19.23 \text{ km}^2$  ( $-5.1\%$ ), while proglacial lake area increased by  $138.19 \pm 1.18 \text{ km}^2$  ( $+81.7\%$ ). The  
469 development and evolution of lake-terminating glacier–proglacial lake systems are predominantly  
470 concentrated along the southern margin of HMA, including the Hindu Kush, Himalayas,  
471 Nyainqentanglha, and Gangdise Mountains.

472 This dataset offers a robust basis for examining spatially heterogeneous glacier responses to climate  
473 change, coupled glacier–lake evolution, glacier hydrological modeling, glacial lake outburst flood  
474 (GLOF) assessment, and water resource management. Nevertheless, further improvements in data quality  
475 remain necessary, particularly in quantifying glacier–lake contact line length, the degree of glacier–lake  
476 contact (e.g., lake depth and subaqueous glacier front depth), and water temperature measurements.

477

478 **Financial support.** This work was funded by the National Key R&D Program of China (Grant No.  
479 2024YFC3013400) and National Science Foundation of China (Grant No. 42361144874).

480

481 **Author contributions.** YL designed the study, developed the methodology, performed analysis, and  
482 wrote the manuscript. QL provided funding, support and supervision. XL, YY and JY produced data and  
483 performed analysis. All other authors discussed and drafted the formulation of the specifications of the  
484 glacial lake inventory in this study. All authors contributed to the final form of the paper.

485 **Competing interests.** The authors declare that they have no conflict of interest.

486

487 **Code and data availability.** Data described in this manuscript can be accessed at Zenodo under  
488 <https://doi.org/10.5281/zenodo.17369580> (Luo and Liu, 2025). The code for proglacial lake ident-if  
489 ication is included in the supplementary materials.

490

491

## Reference

- Benn, D. I., Hulton, N. R. J., and Mottram, R. H.: ‘Calving laws’, ‘sliding laws’ and the stability of tidewater glaciers, *Ann Glaciol*, 46, 123-130, 10.3189/172756407782871161, 2007a.
- Benn, D. I., Warren, C. R., and Mottram, R. H.: Calving processes and the dynamics of calving glaciers, *Earth-Science Reviews*, 82, 143-179, 10.1016/j.earscirev.2007.02.002, 2007b.
- Bolch, T., Menounos, B., and Wheate, R.: Landsat-based inventory of glaciers in western Canada, 1985–2005, *Remote Sens Environ*, 114, 127-137, <https://doi.org/10.1016/j.rse.2009.08.015>, 2010.
- Brun, F., Berthier, E., Wagnon, P., Kaab, A., and Treichler, D.: A spatially resolved estimate of High Mountain Asia glacier mass balances, 2000-2016, *Nat Geosci*, 10, 668-673, 10.1038/NCEO2999, 2017.
- Brun, F., Wagnon, P., Berthier, E., Jomelli, V., Maharjan, S. B., Shrestha, F., and Kraaijenbrink, P. D. A.: Heterogeneous Influence of Glacier Morphology on the Mass Balance Variability in High Mountain Asia, *Journal of Geophysical Research: Earth Surface*, 124, 1331-1345, 10.1029/2018jf004838, 2019.
- Carrivick, J. L. and Tweed, F. S.: Proglacial lakes: character, behaviour and geological importance, *Quaternary Sci Rev*, 78, 34-52, 10.1016/j.quascirev.2013.07.028, 2013.
- Chen, F., Zhang, M., Guo, H., Allen, S., Kargel, J. S., Haritashya, U. K., and Watson, C. S.: Annual 30 m dataset for glacial lakes in High Mountain Asia from 2008 to 2017, *Earth System Science Data*, 13, 741-766, 10.5194/essd-13-741-2021, 2021.
- Chernos, M., Koppes, M., and Moore, R. D.: Ablation from calving and surface melt at lake-terminating Bridge Glacier, British Columbia, 1984–2013, *The Cryosphere*, 10, 87-102, 10.5194/tc-10-87-2016, 2016.
- Foga, S., Scaramuzza, P. L., Guo, S., Zhu, Z., Dilley, R. D., Beckmann, T., Schmidt, G. L., Dwyer, J. L., Joseph Hughes, M., and Laue, B.: Cloud detection algorithm comparison and validation for operational Landsat data products, *Remote Sens Environ*, 194, 379-390, <https://doi.org/10.1016/j.rse.2017.03.026>, 2017.
- Gardelle, J., Berthier, E., and Arnaud, Y.: Slight mass gain of Karakoram glaciers in the early twenty-first century, *Nat Geosci*, 5, 322-325, 10.1038/Ngeo1450, 2012.
- Hanshaw, M. N. and Bookhagen, B.: Glacial areas, lake areas, and snow lines from 1975 to 2012: status of the Cordillera Vilcanota, including the Quelccaya Ice Cap, northern central Andes, Peru, *The Cryosphere*, 8, 359-376, 10.5194/tc-8-359-2014, 2014.
- Hugonnet, R., McNabb, R., Berthier, E., Menounos, B., Nuth, C., Girod, L., Farinotti, D., Huss, M., Dussaillant, I., Brun, F., and Kaab, A.: Accelerated global glacier mass loss in the early twenty-first century, *Nature*, 592, 726-731, 10.1038/s41586-021-03436-z, 2021.
- Kääb, A., Treichler, D., Nuth, C., and Berthier, E.: Brief Communication: Contending estimates of 2003–2008 glacier mass balance over the Pamir–Karakoram–Himalaya, *The Cryosphere*, 9, 557-564, 10.5194/tc-9-557-2015, 2015.
- Khanal, S., Tiwari, S., Lutz, A. F., Hurk, B. V. D., and Immerzeel, W. W.: Historical Climate Trends over High Mountain Asia Derived from ERA5 Reanalysis Data, *Journal of Applied Meteorology and Climatology*, 62, 263-288, <https://doi.org/10.1175/JAMC-D-21-0045.1>, 2023.
- Li, D., Shangguan, D., and Anjum, M. N.: Glacial Lake Inventory Derived from Landsat 8 OLI in 2016–2018 in China–Pakistan Economic Corridor, *ISPRS International Journal of Geo-Information*, 9, 10.3390/ijgi9050294, 2020.

Li, J. and Sheng, Y.: An automated scheme for glacial lake dynamics mapping using Landsat imagery and digital elevation models: a case study in the Himalayas, *Int J Remote Sens*, 33, 5194-5213, 10.1080/01431161.2012.657370, 2012.

Liu, Q., Mayer, C., Wang, X., Nie, Y., Wu, K., Wei, J., and Liu, S.: Interannual flow dynamics driven by frontal retreat of a lake-terminating glacier in the Chinese Central Himalaya, *Earth Planet Sc Lett*, 546, 10.1016/j.epsl.2020.116450, 2020.

Luo, W., Zhang, G., Chen, W., and Xu, F.: Response of glacial lakes to glacier and climate changes in the western Nyainqentanglha range, *Sci Total Environ*, 735, 139607, 10.1016/j.scitotenv.2020.139607, 2020.

Luo, Y. and Liu, Q.: Rapidly Changing Lake-Terminating Glaciers in High Mountain Asia: A Dataset from 1990 to 2022, Zenodo [dataset], <https://doi.org/10.5281/zenodo.17369580>, 2025.

Luo, Y., Yin, Y., Zhong, Y., Lu, X., Yang, J., Sapkota, L., Lu, X., and Liu, Q.: Dynamics of lake-terminating glaciers in the Himalaya and Southeastern Tibet between 1990 and 2020, *Journal of Glaciology*, 1-20, 10.1017/jog.2025.10088, 2025.

Maurer, J. M., Schaefer, J. M., Rupper, S., and Corley, A.: Acceleration of ice loss across the Himalayas over the past 40 years, *Science Advances*, 5, eaav7266, doi:10.1126/sciadv.aav7266, 2019.

Mertes, J. R., Thompson, S. S., Booth, A. D., Gulley, J. D., and Benn, D. I.: A conceptual model of supraglacial lake formation on debris-covered glaciers based on GPR facies analysis, *Earth Surface Processes and Landforms*, 42, 903-914, <https://doi.org/10.1002/esp.4068>, 2017.

Minowa, M., Schaefer, M., and Skvarca, P.: Effects of topography on dynamics and mass loss of lake-terminating glaciers in southern Patagonia, *Journal of Glaciology*, 1-18, 10.1017/jog.2023.42, 2023.

Pronk, J. B., Bolch, T., King, O., Wouters, B., and Benn, D. I.: Contrasting surface velocities between lake- and land-terminating glaciers in the Himalayan region, *The Cryosphere*, 15, 5577-5599, 10.5194/tc-15-5577-2021, 2021.

Quincey, D. J., Richardson, S. D., Luckman, A., Lucas, R. M., Reynolds, J. M., Hambrey, M. J., and Glasser, N. F.: Early recognition of glacial lake hazards in the Himalaya using remote sensing datasets, *Global Planet Change*, 56, 137-152, 10.1016/j.gloplacha.2006.07.013, 2007.

Salerno, F., Thakuri, S., D'Agata, C., Smiraglia, C., Manfredi, E. C., Viviano, G., and Tartari, G.: Glacial lake distribution in the Mount Everest region: Uncertainty of measurement and conditions of formation, *Global Planet Change*, 92-93, 30-39, 10.1016/j.gloplacha.2012.04.001, 2012.

Sherpa, S. F., Smith, L. C., Wang, B., and Stuurman, C.: Brief Communication: Multisource Remote Sensing Detects Growing Himalayan Glacial Lake Outburst Flood Hazards, *EGU sphere*, 2025, 1-9, 10.5194/egusphere-2025-133, 2025.

Shrestha, F., Steiner, J. F., Shrestha, R., Dhungel, Y., Joshi, S. P., Inglis, S., Ashraf, A., Wali, S., Walizada, K. M., and Zhang, T.: A comprehensive and version-controlled database of glacial lake outburst floods in High Mountain Asia, *Earth System Science Data*, 15, 3941-3961, 10.5194/essd-15-3941-2023, 2023.

Shugar, D. H., Burr, A., Haritashya, U. K., Kargel, J. S., Watson, C. S., Kennedy, M. C., Bevington, A. R., Betts, R. A., Harrison, S., and Strattman, K.: Rapid worldwide growth of glacial lakes since 1990, *Nat Clim Change*, 10, 939-945, 10.1038/s41558-020-0855-4, 2020.

Steiner, J., Armstrong, W., Kochtitzky, W., McNabb, R., Aguayo, R., Bolch, T., Maussion, F., Agarwal, V., Barr, I., Baurley, N. R., Cloutier, M., DeWater, K., Donachie, F., Drocourt, Y., Garg, S., Joshi, G., Guzman, B., Kutuzov, S., Loriaux, T., Mathias, C., Menounos, B., Miles, E., Osika, A., Potter, K., Racoviteanu, A., Rick, B., Sterner, M., Tallentire, G. D., Tielidze, L., White, R., Wu, K., and Zheng, W.:

Global mapping of lake-terminating glaciers, *Earth Syst. Sci. Data Discuss.*, 2025, 1-22, 10.5194/essd-2025-315, 2025.

Sugiyama, S., Skvarca, P., Naito, N., Enomoto, H., Tsutaki, S., Tone, K., Marinsek, S., and Aniya, M.: Ice speed of a calving glacier modulated by small fluctuations in basal water pressure, *Nat Geosci*, 4, 597-600, 10.1038/ngeo1218, 2011.

Sutherland, J. L., Carrivick, J. L., Gandy, N., Shulmeister, J., Quincey, D. J., and Cornford, S. L.: Proglacial Lakes Control Glacier Geometry and Behavior During Recession, *Geophysical Research Letters*, 47, 10.1029/2020gl088865, 2020.

Truffer, M. and Motyka, R. J.: Where glaciers meet water: Subaqueous melt and its relevance to glaciers in various settings, *Reviews of Geophysics*, 54, 220-239, 10.1002/2015rg000494, 2016.

Tsutaki, S., Fujita, K., Nuimura, T., Sakai, A., Sugiyama, S., Komori, J., and Tshering, P.: Contrasting thinning patterns between lake- and land-terminating glaciers in the Bhutanese Himalaya, *The Cryosphere*, 13, 2733-2750, 10.5194/tc-13-2733-2019, 2019.

Wang, X., Guo, X., Yang, C., Liu, Q., Wei, J., Zhang, Y., Liu, S., Zhang, Y., Jiang, Z., and Tang, Z.: Glacial lake inventory of high-mountain Asia in 1990 and 2018 derived from Landsat images, *Earth System Science Data*, 12, 2169-2182, 10.5194/essd-12-2169-2020, 2020.

Worni, R., Huggel, C., and Stoffel, M.: Glacial lakes in the Indian Himalayas--from an area-wide glacial lake inventory to on-site and modeling based risk assessment of critical glacial lakes, *Sci Total Environ*, 468-469 Suppl, S71-84, 10.1016/j.scitotenv.2012.11.043, 2013.

Yao, T., Thompson, L., Yang, W., Yu, W., Gao, Y., Guo, X., Yang, X., Duan, K., Zhao, H., Xu, B., Pu, J., Lu, A., Xiang, Y., Kattel, D. B., and Joswiak, D.: Different glacier status with atmospheric circulations in Tibetan Plateau and surroundings, *Nat Clim Change*, 2, 663-667, 10.1038/nclimate1580, 2012.

Zhang, G., Yao, T., Xie, H., Wang, W., and Yang, W.: An inventory of glacial lakes in the Third Pole region and their changes in response to global warming, *Global Planet Change*, 131, 148-157, 10.1016/j.gloplacha.2015.05.013, 2015.

Zhang, G., Zheng, G., Gao, Y., Xiang, Y., Lei, Y., and Li, J.: Automated Water Classification in the Tibetan Plateau Using Chinese GF-1 WFV Data, *Photogrammetric Engineering & Remote Sensing*, 83, 509-519, 10.14358/pers.83.7.509, 2017.

Zhang, G., Bolch, T., Yao, T., Rounce, D. R., Chen, W., Veh, G., King, O., Allen, S. K., Wang, M., and Wang, W.: Underestimated mass loss from lake-terminating glaciers in the greater Himalaya, *Nat Geosci*, 16, 333-338, 10.1038/s41561-023-01150-1, 2023.

Zheng, G., Mergili, M., Emmer, A., Allen, S., Bao, A., Guo, H., and Stoffel, M.: The 2020 glacial lake outburst flood at Jinwuco, Tibet: causes, impacts, and implications for hazard and risk assessment, *The Cryosphere*, 15, 3159-3180, 10.5194/tc-15-3159-2021, 2021a.

Zheng, G., Allen, S. K., Bao, A., Ballesteros-Cánovas, J. A., Huss, M., Zhang, G., Li, J., Yuan, Y., Jiang, L., Yu, T., Chen, W., and Stoffel, M.: Increasing risk of glacial lake outburst floods from future Third Pole deglaciation, *Nat Clim Change*, 11, 411-417, 10.1038/s41558-021-01028-3, 2021b.